*Kidney International, Vol. 61 (2002), pp. 1124–1135*

# In vivo detection of acute rat renal allograft rejection by MRI with USPIO particles

**Qing Ye, Dewen Yang, Mangay Williams, Donald S. Williams, Charnchai Pluempitiwiriyawej, José M.F. Moura, and Chien Ho**

*Department of Biological Sciences, Pittsburgh NMR Center for Biomedical Research, and Department of Electrical and Computer Engineering, Carnegie Mellon University, Pittsburgh, Pennsylvania, USA*

**In vivo detection of acute rat renal allograft rejection by MRI with USPIO particles.**

*Background.* Magnetic resonance imaging (MRI) for non-invasively detecting renal rejection was developed by monitoring the accumulation of macrophages labeled with dextran-coated ultrasmall superparamagnetic iron oxide (USPIO) particles at the rat renal allografts during acute rejection.

*Methods.* Five groups of male rats with DA→BN renal allografts and one group with BN→BN renal isografts were investigated by MRI before, immediately after, and 24 hr after intravenous infusion with different doses of USPIO particles. All infusions were done on post-operative day 4. MRI experiments were carried out in a 4.7-Tesla instrument using a gradient echo sequence.

*Results.* MR signal intensity (MRSI) of the cortex was found to decrease with higher dosages of USPIO particles. In the absence of USPIO infusion, a decrease in MRSI was seen in the medulla region, presumably due to hemorrhage associated with renal graft rejection, while no significant change was observed in the cortex. The optimal dose of USPIO particles for visualizing rejection-associated changes in our rat kidney model appears to be 6 mg Fe/kg body weight. Iron staining results correlated with the MRSI data, indicating that the signal reduction in the MR images was due to the presence of iron. Immunohistochemical results indicated that USPIO particles were mostly taken up by infiltrating macrophages in the rejecting grafts.

*Conclusions.* Our results suggest that MRI with intravenous administration of dextran-coated USPIO particles appears to be a valuable and promising tool that can be used as a non-invasive and sensitive method to detect graft rejection in renal transplantation.

Renal transplantation is a commonly accepted therapeutic modality for treatment of patients with end-stage renal disease. However, long-term graft survival is still threatened by acute and chronic rejection, as well as by complications such as infection and nephrotoxicity caused by immunosuppression [1–3]. Thus, a proper evaluation of the progression of graft rejection could have a significant impact on the management and outcome of transplantation patients. Although numerous techniques have been used for the detection of renal allograft rejection, development of specific, sensitive, and non-invasive methods for the diagnosis of rejection is still a major challenge in the field of renal transplantation. Renal biopsy is generally accepted as the "gold standard" for diagnosing graft rejection. However, this procedure is not only prone to sampling errors, but it also exposes patients to the risks of possible bleeding, kidney rupture, infection, and arterial venous fistula [3, 4].

Magnetic resonance imaging (MRI) is an established methodology for both clinical applications and research in biomedical sciences. Its sensitivity, non-invasiveness, and versatility allow a comprehensive characterization of a disease state. An aspect of particular relevance in the application to transplanted organs is that MRI can be used to detect organ rejection non-invasively, allowing a sequential monitoring of the progression of graft status and its responses to immunosuppression [5]. MR signal intensity (MRSI) is governed by a number of parameters [proton density, relaxation times ($T_1$, $T_2$, $T_2$*), water diffusion, and water exchange rates, etc.] that depend on the physical and physiological properties of the tissue.

Dextran-coated superparamagnetic iron oxide (USPIO) particles are excellent MR contrast agents due to their large magnetic susceptibility produced by iron [6]. Since USPIO particles have an intravascular distribution, a relatively long half life of about two hours in rat blood, and are taken up by macrophages in widespread areas [7, 8], they have been used as a tissue MRI contrast agent [9–13]. In the kidney, USPIO particles also have been used as vascular contrast agents for assessing perfusion rates [14, 15] and as a probe for detecting intrarenal macrophage infiltration [16, 17].

**Key words:** magnetic resonance imaging, ultrasmall superparamagnetic iron oxide particles, macrophages, rat renal transplantation, diagnosis of renal graft rejection.

Received for publication June 14, 2001
and in revised form August 29, 2001
Accepted for publication October 1, 2001

**Table 1.** Experimental design for this study

| Groups | Day 0 KTx D→R | POD 4, 1st MRI 10 min before USPIO infusion | Infuse USPIO *mg Fe/kg* | POD 4, 2nd MRI 5 min after USPIO infusion | POD 5, 3rd MRI 24 hrs after USPIO infusion |
|---|---|---|---|---|---|
| I ($N = 8$) | DA→BN allograft | Three were sacrificed for histology | 0 | | Sacificed for histology, immunohistochemistry |
| II ($N = 5$) | DA→BN allograft | | 1 | | Sacrificed for histology, immunohistochemistry |
| III ($N = 6$) | DA→BN allograft | | 3 | | Sacrificed for histology, immunohistochemistry |
| IV ($N = 7$) | DA→BN allograft | | 6 | | Sacrificed for histology, immunohistochemistry |
| V ($N = 6$) | DA→BN allograft | | 12 | | Sacrificed for histology, immunohistochemistry |
| VI ($N = 8$) | BN→BN isograft | Three were sacrificed for histology | 6 | | Sacificed for histology, immunohistochemistry |

Abbreviations are: KTx, kidney transplantation; D, donor; R, recipient; DA, inbred DA rat strain (RT1$^a$); BN, Brown Norway rat strain (RT1$^n$); POD, post-operative day; MRI, magnetic resonance imaging; USPIO, dextran-coated superparamagnetic iron oxide.

Renal graft rejection is characterized histologically by the infiltration of predominantly T cells and macrophages at the rejection site. Although T-cell infiltration is a hallmark of renal allograft rejection, early and persistent macrophage infiltration is strongly associated with the presence of allograft rejection [18–22]. Thus, it is of interest to develop non-invasive methods using MRI to detect the accumulation of these cells labeled with USPIO particles. A number of studies have shown that sufficient amounts of dextran-coated USPIO particles can be incorporated into cells so that the labeled cells can be detected by MRI [11, 23–25]. Our preliminary results have shown that dextran-coated USPIO particles can be used to detect renal graft rejection by monitoring macrophage infiltration by MRSI reduction [17], but the optimal conditions as well as the cause of MRSI reduction of the renal grafts remain to be determined.

In the present study, we have extended and refined our earlier work to detect the accumulation of macrophages labeled with dextran-coated USPIO particles at the rejecting rat renal graft as a means to detect kidney rejection. Our results are very promising, suggesting that our MRI approach may offer a new non-invasive method to detect rejection in renal transplantation.

## METHODS

### Animals and experimental design

Inbred male DA (RT1$^a$) and Brown Norway (BN, RT1$^n$) rats were purchased from Harlan-Sprague Dawley, Inc. (Indianapolis, IN, USA) at 8 to 10 weeks of age and housed in the animal facility of the Pittsburgh NMR Center for Biomedical Research on a diet of standard rat chow and water ad libitum. Animals received care in compliance with the *Principles of Laboratory Animal Care and the Guide for Care and Use of Laboratory Animals*, published by the National Institutes of Health (NIH publication No. 96-03, revised 1996). Animal protocols were approved by the Institutional Animal Care and Use Committee of Carnegie Mellon University. The present study was performed on six groups of rats (groups I to VI, Table 1). Eight BN rats that received BN kidneys served as an isograft group (group VI). The other 32 BN rats received renal allografts from DA rats and were used as the acute rejection group. Three each from both isograft and allograft recipients were sacrificed on post-operative day (POD) 4 to characterize the pathological condition of the grafts before USPIO infusion. The remaining allograft recipients were divided into five groups (groups I to V, $N = 5$ to 7/group) that were studied by MRI 10 minutes before, 5 minutes after, and 24 hours after infusion with 0 [phosphate-buffered saline (PBS) only], 1, 3, 6, or 12 mg Fe/kg body weight of dextran-coated USPIO particles (or 0, 18, 54, 108 or 216 μmol Fe/kg), respectively. The remaining five isograft recipients underwent the same study with infusion of 6 mg Fe/kg. All USPIO infusions were done on POD 4.

### Renal transplantation

Renal transplantation was performed according to Lee's microsurgical technique [26] with minor modifications. In brief, after nephrectomy on the left side of the recipient, the graft renal artery and vein were anastomosed end-to-side with the recipient abdominal aorta and inferior vena cava, and an end-to-end anastomosis of the ureter was carried out with four single stitches using 10-0 suture (Sherwood Medical, St. Louis, MO, USA). The total ischemic time for the graft was about 25 minutes. The recipient right kidney was kept intact as an internal control for MRI measurements.

### USPIO particles

Dextran-coated USPIO particles were synthesized in our laboratory according to the method of Palmacci and

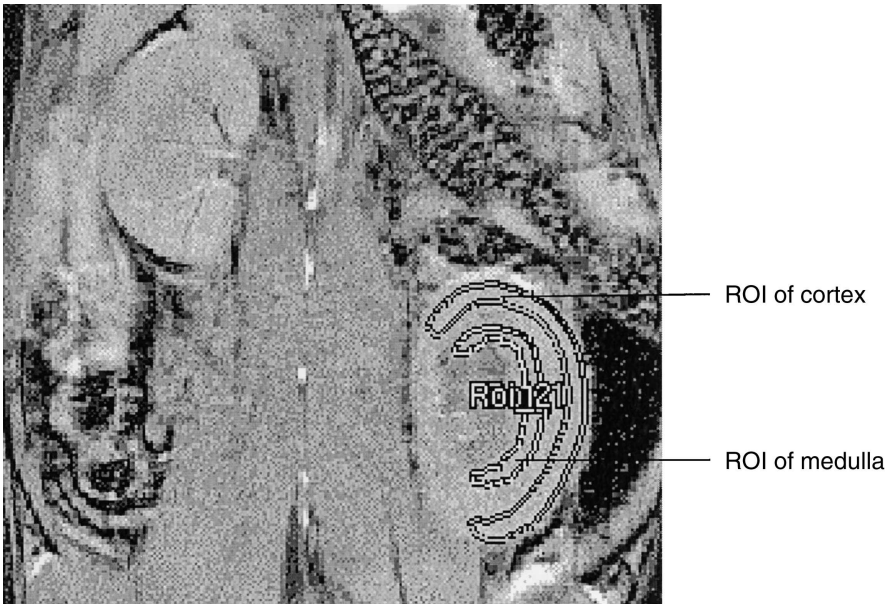


**Fig. 1. Regions of interest (ROIs) for measurements of magnetic resonance (MR) signal intensity.** ROIs for cortex and medulla of kidneys were traced by hand on the center slice of each MRI tested kidney. These ROIs were used to analyze the before- and after-infusion images from all groups of this study.

Josephson [27] with slight modifications [25]. Quantitative determination of iron in the particle suspension was performed for all samples using a spectrophotometric method [28]. Iron-core size measured with transmission electron microscopy (TEM) was found to be in the range 4.0 to 7.5 nm. The mean diameter of whole particles measured by laser light scattering was 27 ± 1.1 nm. The MR relaxivities, $R_1$ (spin-lattice relaxation rate constant, $1/T_1$, per mole of Fe in USPIO) and $R_2$ (spin-spin relaxation rate constant, $1/T_2$, per mole of Fe in USPIO), measured at 0.47 Tesla (20 MHz) using a Bruker Minispec (Bruker Canada, Ltd., Melton, Ont., Canada) at 27.8°C were $3.83 \times 10^4$ and $10.8 \times 10^4$ mol $Fe^{-1}s^{-1}$, respectively. Prior to infusion, a portion of the stock suspension of USPIO particles was dialyzed against PBS, filter sterilized, and assayed for iron content [28]. The USPIO suspensions were diluted with PBS such that a total volume of 1 mL injected intravenously over about two seconds for each individual animal gave the required mg Fe/kg body weight.

### In vivo MRI experiments and MR signal intensity measurement

A 30-cm PE50 extension tube was inserted into the right jugular vein of the recipient for infusing USPIO particles or PBS before MRI. During the MRI experiments, all of the rats were under general anesthesia with 2% isoflurane in a nitrous oxide/oxygen (2:1) mixture using endotracheal intubation and placed in the supine position in the center of the coil. MRI measurements were performed on a Bruker AVANCE DRX MR instrument operating at 4.7 Tesla equipped with a 40-cm horizontal bore superconducting solenoid and a 15-cm shielded gradient insert. Coronal MR images of bilateral kidneys were obtained using a 7-cm diameter Bruker RF coil at 10 minutes before, 5 minutes after, and 24 hours after infusion of USPIO particles. The imaging sequence consisted of a gradient echo sequence with TR/TE = 300/7 ms; flip angle = Ernst angle; FOV = 7 cm; matrix size = 256 × 256; 8 contiguous slices with thickness of 1 mm, three averages; scan time = 3.8 min.

The average changes of MRSI were measured in two different compartments, that is, cortex and medulla in each transplanted kidney. Regions of interest (ROIs) for cortex and medulla were traced manually on the center slice of each kidney (Fig. 1). These ROIs were used to analyze MR images before and after infusion of USPIO particles. MRSI was normalized to that of the psoas major muscle of the same rat. The MRSI reduction in each animal was calculated according to $(SI_1 - SI_2)/SI_1 \times 100\%$, where $SI_1$ and $SI_2$ were the signal intensities before and after USPIO infusion, with both first normalized to the MRSI of the muscle.

### Histological, iron staining, and immunohistochemical analyses

In addition to the six recipients that were sacrificed on POD 4, native and graft kidneys of all recipient rats were harvested immediately after the last MRI measurement on POD 5. The kidneys were fixed in 3.7% paraformaldehyde, embedded in paraffin, and then cut longitudinally into sections of 5-μm thickness with the same coronal orientation as the orientation of the MRI section. In order to correlate the iron distribution with monocyte/macrophage or T-cell locations, serial sections from each sample were stained with hematoxylin and eosin (H&E),

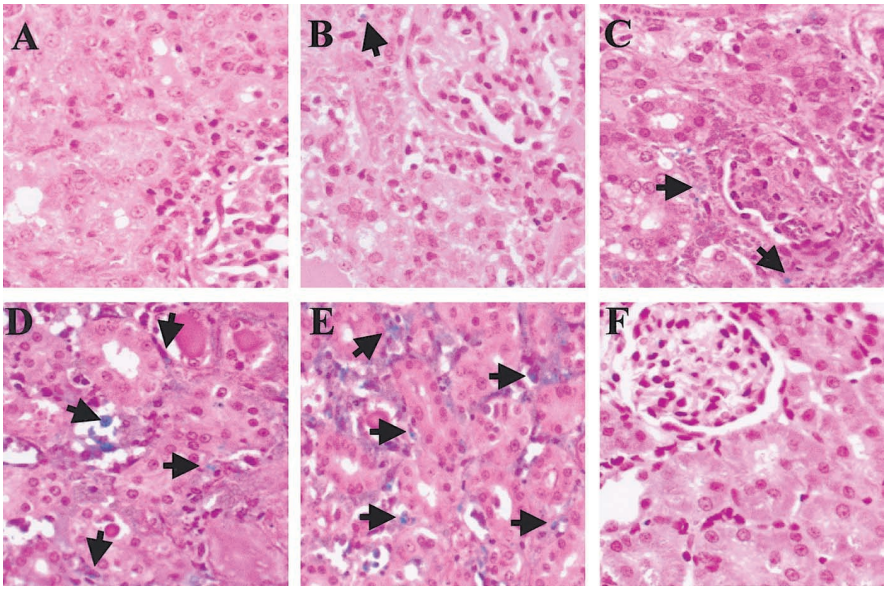


**Fig. 4. Perl's Prussian blue staining at postoperative day (POD) 5, 24 hours after infusion, shows the visible distribution of the iron particles.** *A, B, C, D, E,* and *F* show representative staining of the cortex from groups I, II, III, IV, V, and VI, respectively. Comparing B and C with D and E, there are many more visible iron particles in the latter as indicated by arrows. Almost no visible iron plaques were observed in the isograft (F). Original magnification, ×200. Details are in the text and Table 1.

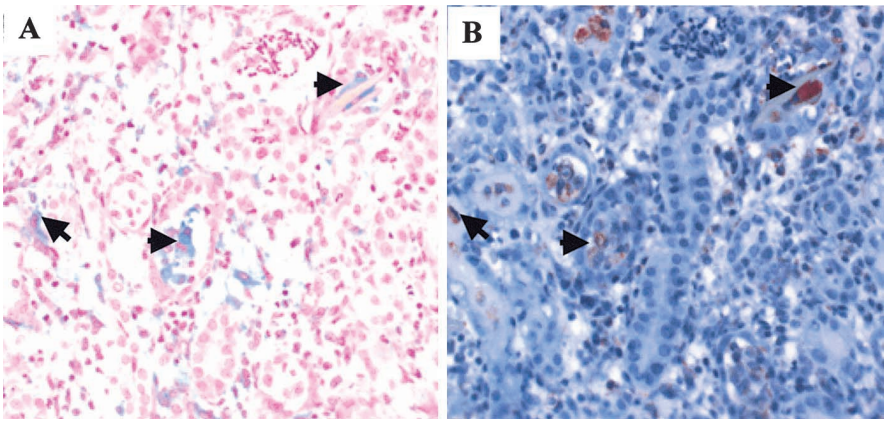


**Fig. 8. Correlation between iron staining and ED1$^+$ cell staining in an allograft.** Representative staining of the cortex of a POD 5 allograft from group IV is shown. (*A*) Iron staining and (*B*) ED1$^+$ cells (monocytes/macrophages). The distribution of the iron-containing cells correlates well with the presence of ED1$^+$ cells as indicated by arrows. Original magnification, ×400. Detailed experimental conditions are in the text and Table 1.

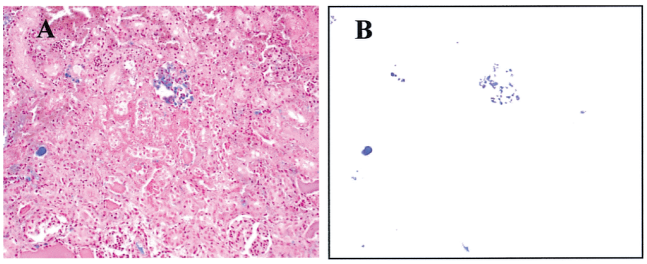


**Fig. 2. Analysis of the Perl's Prussian blue iron staining.** (*A*) An example of the original RGB images of the renal graft. (*B*) The extraction of the Perl's Prussian blue color of the iron stains from the example in panel A. A comparison of the two figures shows that the algorithm extracts the blue color of the iron quite accurately. Details are in the text.

Perl's Prussian blue (iron staining), anti-rat macrophage lineage monoclonal antibodies (ED1; Serotec, Raleigh, NC, USA), and anti-rat T-cell monoclonal antibodies (CD3; DAKO, Carpinteria, CA, USA). All stainings were performed in the Transplantation Pathology Laboratory of the University of Pittsburgh Medical Center in a blind manner. The numbers of ED1$^+$ or CD3$^+$ cells that infiltrated the renal cortex and medulla were counted in a blinded manner as the number of cells per field of view (c/FV) at a magnification of 400×, with five randomly chosen fields/section/rat. Perl's Prussian blue staining for iron was analyzed automatically by summing the luminance of the blue regions in the image of slices stained for iron. The details are described below. Three fields of view were evaluated in a blind manner for each section at a magnification of ×200.

### Analysis of Perl's Prussian blue iron staining

In the renal graft images, the iron stain, which indicates the presence of the USPIO particles, appeared blue in contrast to the background that was purple to magenta. These images were collected in the RGB (red-green-blue) format. To analyze the Perl's Prussian blue iron staining, we started by transforming each of the RGB images into the HSV (hue-saturation-value) coordinate system. The HSV color space was chosen over the RGB format because the RGB format, though commonly used for display, was not perceptually uniform. In the HSV format, hue describes the specification of the basic color in terms of its angular position on the "color wheel." As hue varies from 0 to 1.0 (or 360°), the corresponding color changes from red to yellow, green, cyan, blue, magenta and back to red again. Saturation indicates the purity of the color. A color appears dull (or gray) at low saturation, and it becomes increasingly vivid at higher saturation levels. The last component of the HSV color space is the value, often also referred to as the brightness, which represents the degree of intensity of the light.

After transforming the RGB image into the HSV color space, the blue color was then extracted in the image by thresholding. A certain range of the hue components of the HSV image was chosen. Although the typical hue range for the blue color was between 0.6 and 0.75, in our algorithm these thresholds were adjustable by the expert user, since different image slides had varying brightness intensity and the choice of blue in each of the slides was subjective. In some of these slides where the brightness intensity was low, the expert user was sometimes not able to differentiate the dark blue pixels from the dark purple ones. This problem was resolved by a non-linear filter operation: median filtering. This median filtering filtered out possible false dark purple pixels: a 5 by 5 window was sliced through each of the blue pixel candidates obtained from the previous step; this pixel was kept if there were more blue pixels than purple pixels in the 5 by 5 window.

Finally, for display purposes, these true blue pixels were transformed back into the RGB space, and all the luminance values of all the true blue pixels were summed. The luminance value (Y) is given by [29]

$$Y = 0.177\ R + 0.813\ G + 0.011\ B \quad \text{(Eq. 1)}$$

where R, G, and B are the intensities of the red, green, and blue components of the image, respectively. Figure 2A depicts an example of the original RGB images of the renal graft with 12 mg Fe/kg USPIO infusion. Figure 2B shows the extraction of the Perl's Prussian blue color of the iron stains from Figure 2A. This figure clearly indicates that the algorithm extracts the blue color of the iron quite accurately.

### Statistical analysis

Data from this study were expressed as mean ± SD. Differences between groups were identified using ANOVA with the Bonferroni multiple comparisons post-test. *P* values less than 0.05 were considered significant.

## RESULTS

### In vivo MRI experiments on renal grafts

Recipients from six groups of rats (Table 1) were examined by MRI 10 minutes before, 5 minutes after, and 24 hours after intravenous infusion with 0 (PBS only), 1, 3, 6, or 12 mg Fe/kg body weight of dextran-coated USPIO particles. Representative MR images of rat kidney grafts from this study are shown in Figure 3. In the absence of USPIO infusion (that is, infused with PBS), a decrease in MRSI was seen in the allograft medulla regions, presumably due to hemorrhage associated with renal graft rejection, while no significant change was observed in the cortex (Fig. 3C). We have probed the MRSI changes in the cortex using a dose-dependent response to the USPIO particles on POD 5. MRSI decreases with dosages of USPIO particles from 0 to 12 mg Fe/kg of body weight (Table 2; Figures 3C, F, I, L, and O). The MRSI in the allograft medulla regions shows no clear difference among the five groups after infusion of various doses of USPIO particles on POD 5. Based on these results, 6 mg Fe/kg appears to be the optimal dosage for the visualization of rejection-associated changes in the renal cortex. Figure 3L shows MR images of an allograft at 24 hours after infusion of 6 mg Fe/kg of USPIO particles, and Figure 3R shows images of an isograft under the same conditions. While a significant darkening is seen in the allografts, no significant change in MRSI is observed in the isografts.

### Iron staining of renal grafts

Representative images of Perl's Prussian blue staining of the cortex from kidney grafts of this study are shown in Figure 4. Iron staining in the cortex of allografts after infusion of 6 or 12 mg Fe/kg of USPIO particles (Figs. 4D and E) shows much more dense and more widespread staining than is exhibited in lower dosages of USPIO (Figs. 4B and C). There is no visible iron staining in the cortex of the allografts from group I (Fig. 4A), that is, infused with PBS only. Iron staining in the medulla does not show much difference among five allograft groups (results not shown) after infusion of various doses of USPIO particles; the darkening of the medulla in the MR imaging is believed to be due to hemorrhage. There are no visible iron particles in the cortex of the isografts (Fig. 4F) at 24 hours after infusion of 6 mg Fe/kg of USPIO particles.

Table 2 summarizes the results of MRSI reduction

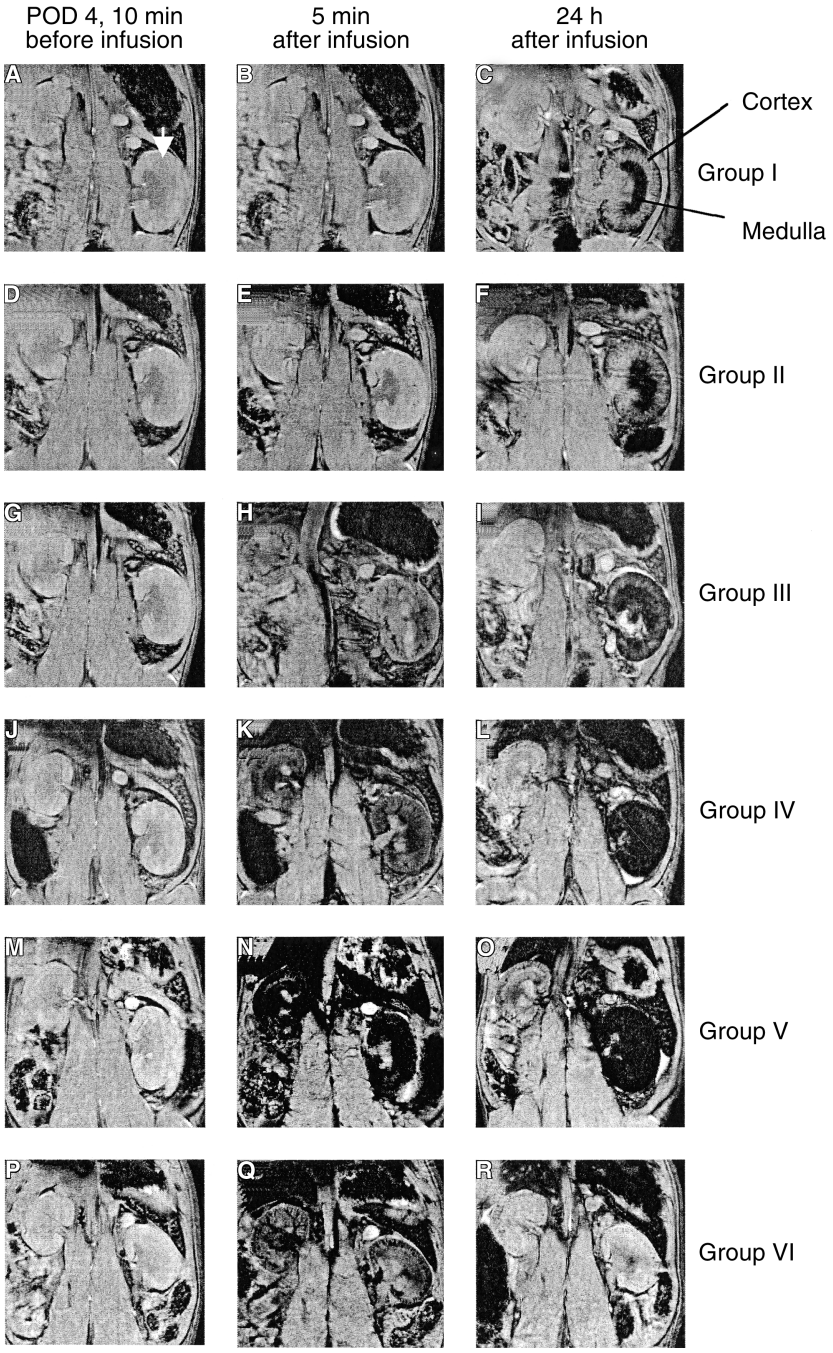


**Fig. 3. Representative gradient-echo MR images showing the effect of different doses of dextran-coated ultrasmall superparamagnetic iron oxide (USPIO) particle infusion.** The transplanted kidneys appear on the right (arrow) and the native kidneys appear on the left in these panels. The images from immediately before, 5 minutes after, and 24 hours after infusion of USPIO particles are shown in the first, second, and third columns, respectively. Allograft images *A*, *B*, and *C* are from group I without USPIO infusion (infused with PBS only); *D*, *E*, and *F* are from group II with 1 mg Fe/kg; *G*, *H*, and *I* are from group III with 3 mg Fe/kg; *J*, *K*, and *L* are from group IV that with 6 mg Fe/kg; and *M*, *N*, and *O* are from group V with 12 mg Fe/kg. *P*, *Q*, and *R* show isograft images from group VI with 6 mg Fe/kg. MR images of the coronal view of the grafts are shown in each case. For details, see the text and Table1.

and intensity of iron staining of cortex at 24 hr after infusion of different dosages of dextran-coated USPIO particles. Analyses show a statistically significant MRSI reduction in the cortex of renal allografts at POD 5, 24 hours after an infusion of 6 or 12 mg Fe/kg of USPIO particles compared to rats infused with 0, 1 or 3 mg Fe/kg ($P < 0.001$). MRSI changes in the medulla of allografts show no statistical difference among the five groups after infusion of various doses of USPIO particles ($P > 0.23$). However, MRSI in the cortex and medulla of renal grafts shows a significant difference between allografts and isografts 24 hours after an infusion of 6 mg Fe/kg of USPIO particles ($P < 0.0001$). MRSI reduction appears to level off above 6 mg Fe/kg, and this dosage of USPIO appears to be an optimal one for the chosen MRI pulse sequence. In a separate experiment to determine the dynamic behavior of MRSI after a bolus USPIO infusion, we have also found that a dose of 6 mg Fe/kg gives a reproducible wash-in/wash-out curve [30].

Our iron staining analysis indicates that there is some

**Table 2.** MR signal intensity reduction and iron staining of kidney grafts 24 hours after infusion of USPIO particles on POD 5

| Group | *N* | USPIO *mg Fe/kg* | MRSI[a] reduction % | | Iron staining[b] *arbitrary units* | |
|---|---|---|---|---|---|---|
| | | | Cortex | Medulla | Cortex | Medulla |
| I | 5 | 0 | 47.56 ± 7.05 | 79.56 ± 3.81 | 1.08 ± 0.67 | NA[g] |
| II | 5 | 1 | 52.72 ± 5.83 | 78.30 ± 3.68 | 18.14 ± 4.96 | NA[g] |
| III | 6 | 3 | 68.03 ± 4.48 | 81.11 ± 5.39 | 303.67 ± 50.40[c] | NA[g] |
| IV | 7 | 6 | 84.54 ± 1.91[c,d] | 84.40 ± 3.16 | 951.85 ± 78.06[c,d] | NA[g] |
| V | 6 | 12 | 86.99 ± 4.19[c,d] | 86.01 ± 4.41 | 1297.35 ± 288.56[c,d] | NA[g] |
| VI | 5 | 6 | 16.00 ± 9.20[e] | 9.70 ± 5.50[e] | 29.61 ± 18.95[f] | 10.24 ± 5.45 |

[a] The MRSI values from all groups in this study are represented as mean ± SD
[b] The iron staining values from all groups in this study are presented as mean ± SD
[c] $P < 0.0001$ vs. Groups I and II
[d] $P < 0.001$ vs. Group III
[e] $P < 0.0001$ vs. Groups I, II, III, and IV
[f] $P < 0.0001$ vs. Groups III, IV, and V
[g] NA, no data analysis available; due to hemorrhage in the medulla, there is no visible difference in the iron staining of the medulla among the five allograft groups

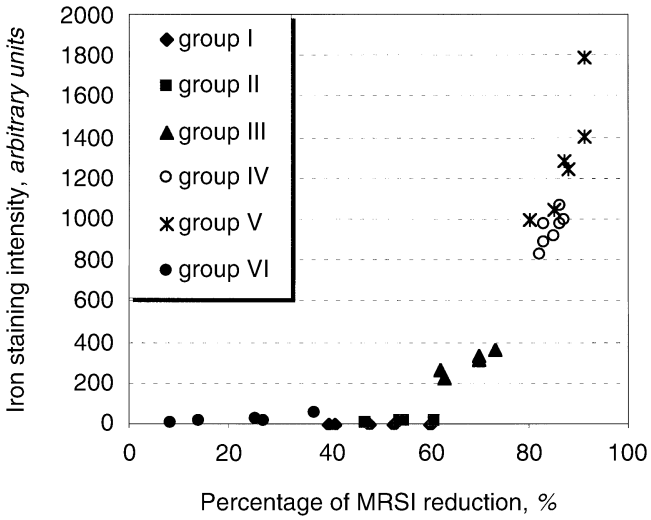


**Fig. 5. Correlation between MRSI reduction and iron staining intensity in the cortex of renal grafts.** The data of MRSI changes and iron staining intensity are shown as percentage and arbitrary units, respectively. For detailed experimental conditions, see the text and Table 1.

iron staining in the cortex and medulla of the isografts (group VI). However, the intensity is significantly lower than in the allografts (group IV) 24 hours after an infusion of the same dose (6 mg Fe/kg) of USPIO particles (Table 2, $P < 0.0001$). Iron staining intensity in the cortex of allografts exhibits significant differences among the five groups (Table 2, $P < 0.0001$), but the iron staining intensity is difficult to detect in the medulla of allografts at 24 hours after infusion of different doses of USPIO, presumably due to a massive hemorrhage (Fig. 3C and Fig. 7B). Although there is a possible overlap between the MRSI reduction caused by the presence of iron and by hemorrhage in allografts on POD 5, the iron staining intensity results from the cortex of allografts match the MRSI data, confirming that the signal reduction in the MR images is predominantly due to the presence of iron. Figure 5 shows the relation between the intensity of iron staining and the percentage of MRSI reduction due to USPIO particles. There is a good correlation between these two sets of data.

### Histological analyses of the renal grafts

Hematoxylin and eosin staining of renal grafts shows that the morphological alteration appears as acute rejection Grade II [31] in all three allografts harvested on POD 4. It is characterized by graft enlargement, entire interstitial infiltration by mononuclear inflammatory cells (particularly in or around glomeruli and the perivascular area), foci of moderate or severe tubulitis, and mild intimal arteritis (Figs. 6A and B). By POD 5, all five groups of allografts were in acute rejection Grade III [31]. In addition to the above morphological changes on POD 4, all renal allografts at POD 5 were enlarged, exhibited heavy interstitial infiltration, severe intimal arteritis, and edematous or necrotic tubular cells. Extensive interstitial hemorrhage was found in the medulla and diffuse interstitial hemorrhage was seen in the cortex (Figs. 7A and B). In contrast, the morphology of isografts harvested on POD 4 (Figs. 6C and D) or POD 5 (Figs. 7C and D) is well preserved, with only minor perivascular and minimal focal interstitial infiltration, and light dilatation of renal tubules.

### Immunohistochemistry of the renal grafts

The immunohistochemical results of the renal grafts have revealed that there were no significant variations in the numbers of $ED1^+$ cells and $CD3^+$ cells among the five allograft groups, but there was a remarkable difference between isograft and allograft at POD 5 ($P < 0.0001$, Table 3). The distribution of $ED1^+$ and $CD3^+$ infiltrates in the renal allografts harvested at POD 5 was similar among the five groups. A dense infiltration of $ED1^+$ and $CD3^+$ cells was observed in the cortex of all allografts. They particularly accumulated in or around glomeruli, vessels, and tubules. However, less staining intensity of $ED1^+$ and $CD3^+$ cells was observed in the necrotic regions of POD 5 allografts, and there was a decrease in the accumulation of these cells, especially

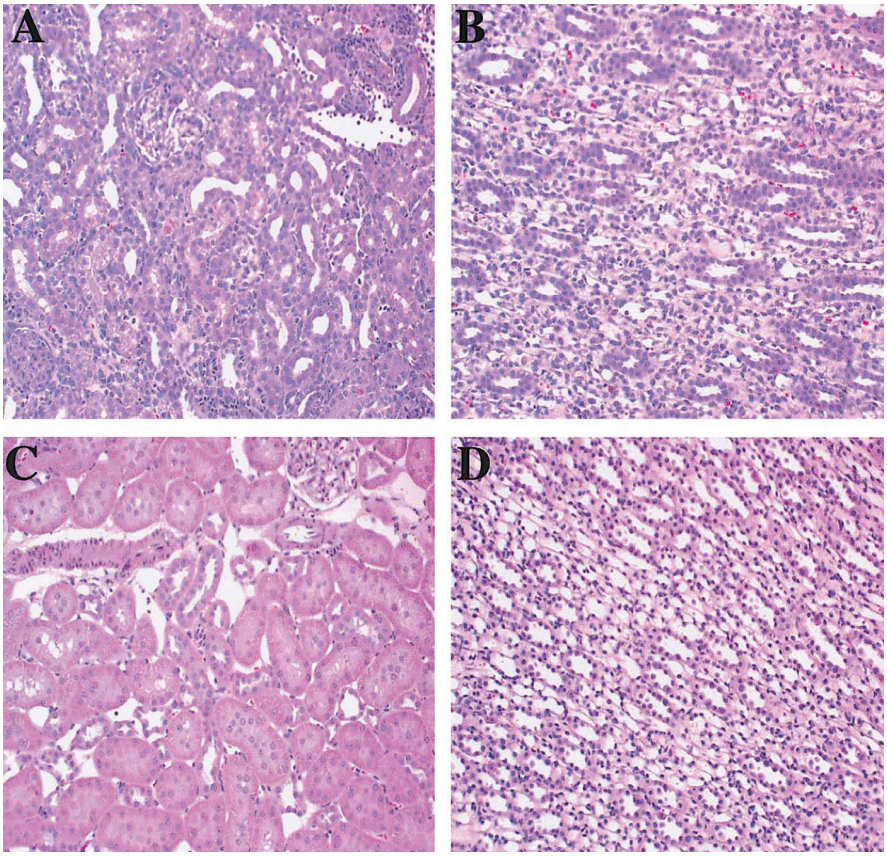


**Fig. 6. Hematoxylin and eosin (H&E) staining shows the pathological changes of POD 4 renal grafts.** Representative optical microscopy images of H&E staining of grafts from groups I and VI are shown. The morphological alteration of the allografts (*A* for cortex and *B* for medulla) appears as acute rejection grade II [31]. The morphology of the isografts (*C* for cortex and *D* for medulla) was well preserved. They exhibited only small perivascular and very mild diffusing interstitial infiltration, and light dilatation of renal tubules. Original magnification, ×100. Detailed experimental conditions are in the text and Table 1.

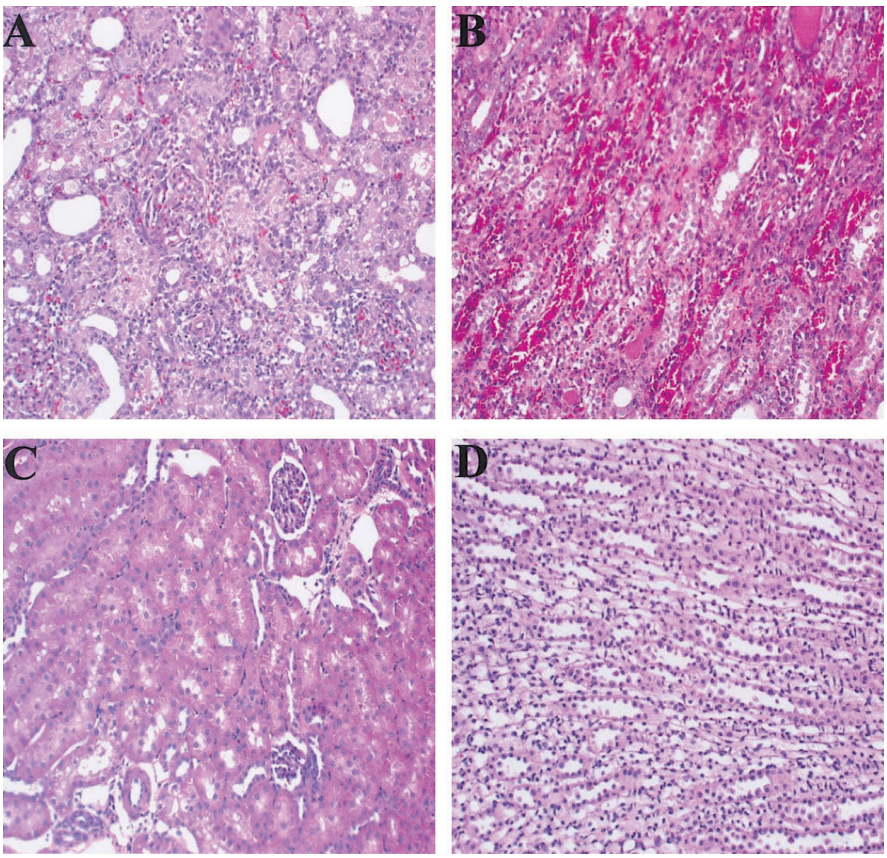


**Fig. 7. H&E staining shows the pathological changes of POD 5 renal grafts.** Representative images of staining of grafts from groups IV and VI are shown. Allografts (*A* for cortex and *B* for medulla) were in acute rejection grade III [31]. In addition to the morphological changes on POD 4, all renal allografts exhibited heavy interstitial infiltration, severe intimal arteritis, and edematous or necrotic tubular cells. Extensive interstitial hemorrhage was found in the medulla, and diffusing interstitial hemorrhage was seen in the cortex. In contrast, the morphology of the isografts (*C* for cortex and *D* for medulla) was well preserved. Original magnification, ×100. Detailed experimental conditions are in the text and Table 1.

**Table 3.** Histology and immunohistochemistry of kidney grafts at POD 5

| Group | Hemorrhage[a] | | ED1$^+$ Cells (C/FV 400x)[b] | | CD3$^+$ Cells (C/FV400x)[b] | |
|---|---|---|---|---|---|---|
| | Cortex | Medulla | Cortex | Medulla | Cortex | Medulla |
| I | + | +++ | 138.73 ± 7.98 | 110.20 ± 7.20 | 98.47 ± 4.93 | 84.73 ± 4.13 |
| II | + | +++ | 141.26 ± 10.63 | 109.67 ± 5.85 | 98.80 ± 7.07 | 82.20 ± 4.84 |
| III | + | +++ | 139.72 ± 7.46 | 108.67 ± 5.59 | 100.22 ± 5.61 | 83.78 ± 4.76 |
| VI | + | +++ | 141.48 ± 5.95 | 107.81 ± 6.24 | 100.29 ± 5.26 | 84.14 ± 4.61 |
| V | + | +++ | 142.78 ± 6.67 | 108.94 ± 8.17 | 99.44 ± 5.58 | 84.78 ± 4.07 |
| VI | − | − | 16.00 ± 6.24[c] | 14.80 ± 3.49[c] | 9.20 ± 1.92[c] | 7.60 ± 1.52[c] |

[a] −, +, and +++, none, diffusing or extensive interstitial hemorrhage seen in the grafts, respectively
[b] The number of cells is presented as mean ± SD
[c] $P < 0.0001$ vs. groups I, II, III, IV, and V

CD3$^+$ cells, in the medulla. In contrast to allografts, there was only very minor diffuse ED1$^+$ and CD3$^+$ cell infiltration and no obvious difference in distribution of ED1$^+$ and CD3$^+$ cells in isografts at POD 5 (results not shown). Figure 8 indicates that the distribution of USPIO particles (Fig. 8A, iron staining) is well correlated with the macrophage infiltration in the cortex of the rejecting allografts (Fig. 8B, ED1$^+$ staining). Some discrepancies between these two types of staining are observed. This may be due to the fact that they were performed on separate histological sections.

## DISCUSSION

Several MRI techniques have been applied for the determination of renal allograft rejection in experimental animal models [32–35] as well as in human studies [36–42]. Most of these early MRI studies focused on functional MRI, while some of them evaluated the graft status by analyzing the anatomical changes of renal allograft based on the loss of corticomedullary differentiation on $T_1$-weighted images [32, 41]. In many aspects, these findings were non-specific, because they could be seen in acute tubular necrosis and cyclosporine toxicity [36, 38]. Beckman et al have reported that DA→Lewis rat kidney allografts could be analyzed by $T_1$- and $T_2$-weighted spin-echo images and bolus-tracking perfusion assessment [14]. MRI anatomical scores (range 1 to 6) and perfusion rates were compared with graft histology (range of rejection score 1 to 6). Both in the acute and chronic phases, the MRI scores correlated significantly with the histological scores, and the perfusion rates also correlated significantly with the MRI score or the histological score. These MRI scores were derived from morphological images, which showed transverse sections of transplanted kidneys in comparison to the contralateral native kidney.

Cell-specific imaging is an increasingly important field of MR imaging [10–13, 16, 17]. It is well known that both T-cells and macrophages are involved in the process of acute renal allograft rejection [17–22]. Although T-cell–rich interstitial nephritis is a hallmark of acute allograft rejection, macrophages and their associated products may influence initial and late changes, and may be more important to the process than previously believed [19–22]. Hence, our current method, which can provide sequential monitoring of the distribution and intensity of infiltrates in the allograft may be more specific and sensitive than other methods used to detect graft rejection.

The use of dextran-coated USPIO particles as a tissue-specific MRI contrast agent is well established [6–17]. It also has been shown that intravenously injected USPIO particles have a great advantage in cell-specific labeling for MRI studies. First, the cell labeling procedure is very simple. Second, labeling through endocytosis and/or phagocytosis does not affect the functional properties of the cells [7, 11, 24]. Renal acute rejection is pathologically characterized by mononuclear cell infiltration in the interstitium, arteritis, and tubulitis [32]. Several studies have reported that the peak of infiltrates in this DA→BN rat acute renal rejection model is about POD 5, and these infiltrates are mostly macrophages and T-cells [17, 43]. Our data have confirmed these observations (Table 3). Weissleder et al demonstrated that 24 hours after intravenous injection in rats, all USPIO particles were accumulated in the macrophages [7]. In their study, lymph node relaxation times decreased maximally within 24 to 48 hours after intravenous administration of USPIO. The $T_2$ of normal lymph nodes had significantly decreased 24 hours after administration. Other groups obtained similar results [12, 13, 16, 17]. Dousset et al demonstrated that MR signal intensity did not change within 4 to 6 hours after intravenous administration of USPIO (AMI-227) even at high doses (17 mg Fe/kg or 300 μmol/kg) [12]. They indicated that the time lapse between intravenous injection and MRSI change is an important parameter that must be established to exceed the blood phase of the free contrast agent molecules, and to allow sufficient time for the iron particles to accumulate within the macrophage phagolysosomes. Our study also has confirmed that the USPIO particles are mostly accumulated in mac-

rophage phagolysosomes 24 hours after infusing with USPIO. We compared the MRSI reduction between pre-infusion at POD 4 and 24 hours after infusion at POD 5.

Organ biodistributions of USPIO particles are widely different. Twenty-four hours after intravenous administration of USPIO particles, 2.9%, 3.6%, 6.3%, and 7.1% of the injected dose per gram of tissue was found in bone marrow, lymph nodes, liver, and spleen of normal rats, respectively [7, 23]. Doussel et al reported that the half life of the USPIO particle (AMI-227) with a dose of 16.8 mg Fe/kg was about 5 to 6 hours in rat blood [12]. Their results indicated that with a high dose (16.8 mg Fe/kg) of AMI-227, EAE rats showed signal intensity decrease related to iron-coated macrophages in the central nervous system, but no signal changes were found after a low dose (2.5 mg Fe/kg) was given. In our results, significant MRSI reduction in the allografts at POD 5 was observed 24 hours after an infusion of 6 or 12 mg Fe/kg of USPIO particles, but no statistically significant change was obtained when less than 3 mg Fe/kg was given. In another study, we used different dosages of USPIO to test USPIO-enhanced dynamic MRI in normal rat [30]. We observed that well-shaped first-pass dynamic curves are observed only for the doses of 3 and 6 mg Fe/kg in the cortex and the latter dosage gave a smaller deviation and a clearer signal intensity reduction. The dynamic curves appeared more rounded and recovery was delayed after maximum signal intensity reduction at the dosage of 12 mg Fe/kg. These data indicate that USPIO particles are cleared from kidney vessels in a time-dependent and dose-dependent fashion. Our immunohistochemical data show no significant difference in number of $ED1^+$ and $CD3^+$ cells among the five renal allograft groups (Table 3). However, there are remarkable differences in the MRSI reduction and iron staining intensity between high and low doses of USPIO administered. Thus, it is likely that with a higher dose of USPIO particles, the particles remain in the blood phase longer, and there is sufficient time for them to be taken up by circulating macrophages/monocytes and/or transported slowly across the capillary endothelium to the interstitium.

The present study shows that MRSI reduction is significantly different in the cortex at different doses, but no statistical difference was found in the medulla among five allograft groups studied (Table 2). The MRSI change also is correlated with the iron staining intensity in the cortex, but not in the medulla (results not shown). These differences might be due to the blood supply and to the fact that macrophage infiltration occurs more in the cortex than in the medulla at POD 5. After intravenous injection, the USPIO particles are distributed in the kidneys probably through several pathways. They may be taken up by circulating macrophages/monocytes and then these cells are attracted to rejecting grafts. The particles may be directly delivered to the interstitium by transcytosis through high endothelial venules in the kidney [7]. They may also move across the ruptured vessels that may be caused by a rejection reaction and diffuse into the interstitium. Those free particles accumulated in the interstitium may then be taken up by infiltrates in the rejecting site and/or are gradually cleared through afferent lymphatic vessels. On POD 5, allografts show Grade III acute rejection, arteritis becomes more severe**,** artery lumina are narrowed and/or are obstructed, and vessels are ruptured. Therefore, diffuse hemorrhage in the cortex and extensive hemorrhage in the medulla are shown in allografts on POD 5 (Fig. 7 A, B). Because of low or no blood flow in severely rejecting grafts [35], the particles distributed to the medulla are much less than those to the cortex. Severe hemorrhage in the medulla causing the MRSI reduction is not significantly different among five allograft groups under different doses or without USPIO administration (Table 2). The effects of hemorrhage on the MRSI reduction may be distinguished by using group I (only PBS infused) as background reference (Fig. 3C).

Magnetic resonance imaging has the capability of detecting both tissue anatomic features and functional status of the graft. USPIO particles have a relatively long half-life in blood (about 2 hours in rats), an intravascular distribution, and can be taken up by infiltrates in allografts. Our present study has shown that a dose of 6 mg Fe/kg of dextran-coated USPIO particles gives good reduction of the MR signal and minimum standard deviation. By using a dose of 6 mg Fe/kg of USPIO particles, perfusion characteristics of the renal graft can also be shown by dynamic MRI [30]. Hence, measurements of renal perfusion followed by detection of macrophage infiltration by MRI after a single administration of dextran-coated USPIO particles appear to be a useful and accurate method to monitor the graft status. This approach also may differentiate graft rejection from CsA nephrotoxicity, acute tubulopathy, and kidney infection when dealing with clinical parameters. We plan to carry out further studies combining dynamic MRI and in vivo cell-labeling MRI to monitor renal rejection by infusion of dextran-coated USPIO particles.

In summary, our results indicate that there is a good correlation between MRSI reduction and the distribution of USPIO in the cortex, and that the optimal dose of dextran-coated USPIO particles to detect the accumulation of the macrophages at the rejecting kidney is about 6 mg Fe/kg body weight in our rat model. Hemorrhage in renal grafts (such as, in the medulla) influences the MRI signal intensity. In conclusion, our results show that detecting rat renal acute rejection with MRI following an intravenous administration of dextran-coated USPIO particles appears to be a valuable and promising tool

that is non-invasive and sensitive with the potential of clinical applications to detect renal graft rejection in transplanted patients.

## ACKNOWLEDGMENTS

This work is supported by research grants from the National Institutes of Health (R41RR-03631 and R01RR/AI-15187). The experiments were performed in the Pittsburgh NMR Center for Biomedical Research, which is supported by a grant (P41RR-03631) from the National Center for Research Resources as an NIH-supported Resource Center. Preliminary results were presented at the Joint Annual Meeting ISMRM and ESMRMB, April 21-27, 2001, Glasgow, Scotland, UK and at the Annual Meeting of the American Society of Transplantation, May 11-16, 2001, Chicago, IL. We wish to thank Dr. Yi-Jen Lin Wu, Ms. Kristy S. Hendrich, Dr. Ming Qiang Huang, Dr. Shinichi Kanno, and Dr. E. Ann Pratt for helpful discussions, and Ms. Elena Simplaceanu for valuable MRI technical suggestions.

*Reprint requests to Dr. Chien Ho, Department of Biological Sciences, Carnegie Mellon University, 4400 Fifth Avenue, Pittsburgh, Pennsylvania 15213-2683, USA.*
*E-mail: chienho@andrew.cmu.edu.*

## REFERENCES

1. Gaber LW, Moore LW, Gaber AO, *et al*: Utility of standardized histological classification in the management of acute rejection. *Transplantation* 65:376–380, 1998
2. Cecka JM: *The UNOS Scientific Renal Transplant Registry*. Clinical Transplants, UCLA Tissue Typing Lab, Los Angeles, CA, USA, 1999, pp 1–21
3. Racusen LC, Solez K, Burdick JF, (editors): *Kidney Transplant Rejection: Diagnosis and Treatment*. New York, Marcel Dekker, Inc, 1998
4. Foster MC, Morgan AG, Wenham PW, *et al*: The late results of renal transplantation and the importance of chronic rejection as a cause of graft loss. *Ann R Coll Surg Engl* 71:44–47, 1989
5. Nicolau B, Hof RP, Rudin M: The role of magnetic resonance imaging and spectroscopy in transplantation: From animal models to man. *NMR Biomed* 13:329–348, 2000
6. Chambon C, Clement O, Le Blanche A, *et al*: Superparamagnetic iron oxides as positive MR contrast agents: *in vitro* and *in vivo* evidence. *J Magn Reson Imaging* 11:509–519, 1993
7. Weissleder R, Elizondo G, Wittenberg J, *et al*: Ultrasmall superparamagnetic iron oxide: Characterization of a new class of contrast agents for MR imaging. *Radiology* 175:489–493, 1990
8. Weissleder R, Hahn PF, Stark DD, *et al*: Superparamagnetic iron oxide: Enhanced detection of focal splenic tumors with MR imaging. *Radiology* 169:399–403, 1988
9. Majumdar S, Zoghbi SS, Gore JC: Pharmacokinetics of superparamagnetic iron-oxide MR contrast agents in the rat. *Invest Radiol* 25:771–777, 1990
10. Anzai Y, Blackwell KE, Hirschowitz SL, *et al*: Initial clinical experience with dextran-coated superparamagnetic iron oxide for detection of lymph node metastases in patients with head and neck cancer. *Radiology* 192:709–715, 1994
11. Yeh TC, Zhang W, Ildstad ST, Ho C: In vivo dynamic MRI tracking of rat T-cells labeled with superparamagnetic iron-oxide particles. *Magn Reson Med* 33:200–208, 1995
12. Dousset V, Gomez C, Petry KG, *et al*: Dose and scanning delay using USPIO for central nervous system macrophage imaging. *Magn Reson Mater Phys Bio Med* 8:185–189, 1999
13. Kanno S, Lee PC, Dodd SJ, *et al*: A novel approach using magnetic resonance imaging for the detection of lung allograft rejection. *J Thorac Cardiovasc Surg* 120:923–934, 2000
14. Beckmann N, Joergensen J, Bruttel K, *et al*: Magnetic resonance imaging for the evaluation of rejection of kidney allograft in the rat. *Transplant Int* 9:175–183, 1996
15. Laissy JP, Idée JM, Loshkajian A, *et al*: Reversibility of experimental acute renal failure in rats: Assessment with USPIO-enhanced MR imaging. *Magn Reson Imaging* 12:278–288, 2000
16. Hauger O, Delalande C, Trillaud H, *et al*: MR imaging of intrarenal macrophage infiltration in an experimental model of nephrotic syndrome. *Magn Reson Med* 41:156–162, 1999
17. Zhang Y, Dodd SJ, Hendrich KS, *et al*: MRI detection of rat renal transplant rejection by monitoring macrophage infiltration. *Kidney Int* 58:1300–1312, 2000
18. Nadasdy T, Krenacs T, Kalmar KN, *et al*: Importance of plasma cells in the infiltration of renal allografts: An immunohistological study. *Path Res Pract* 187:178–183, 1991
19. Paul LC, Grothman GT, Benediktsson H, *et al*: Macrophage subpopulations in normal and transplanted heart and kidney tissue in the rat. *Transplantation* 53:157–162, 1992
20. Nagano H, Nadeau KC, Takada M, *et al*: Sequential cellular and molecular kinetics in acutely rejecting allografts in rats. *Transplantation* 63:1101–1108, 1997
21. Orosz CG, Vanbuskirk AM: Immune mechanisms of acute rejection. *Transplant Proc* 30:859–861, 1998
22. Grau V, Herbst B, Steiniger B: Dynamics of monocytes/macrophages and T lymphocytes in acute rejecting rat renal allografts. *Cell Tissue Res* 291:117–126, 1998
23. Weissleder R, Elizondo G, Wittenberg J, *et al*: Ultrasmall superparamagnetic iron oxide: An intravenous contrast agent for assessing lymph nodes with MR imaging. *Radiology* 175:494–498, 1990
24. Yeh TC, Zhang W, Ildstad ST, Ho C: Intracellular labeling of T-cells with superparamagnetic contrast agents. *Magn Reson Med* 30:617–625, 1993
25. Dodd SJ, Williams M, Suhan JP, *et al*: Detection of single mammalian cells by high-resolution magnetic resonance imaging. *Biophys J* 76:103–109, 1999
26. Lee S: An improved technique of renal transplantation in the rat. *Surgery* 6:771–775, 1967
27. Palmacci S, Josephson L: *Synthesis of Polysaccharide Covered Superparamagnetic Oxide Colloids.* U.S. patent, 5262176. Example 1. November 16, 1993
28. Papisov MI, Bogdanov A Jr, Schaffer B, *et al*: Colloidal magnetic resonance contrast agents: Effect of particle surface on biodistribution. *J Magnetism Magn Mater* 122:383–386, 1993
29. Jain A: *Fundamentals of Digital Image Processing*. New York, Prentice-Hall, Inc, 1989, pp 66–67
30. Yang D, Ye Q, Williams M, *et al*: USPIO-enhanced dynamic MRI: Evaluation of normal and transplanted rat kidneys. *Magn Reson Med* 46:1152–1163, 2001
31. Racusen LC, Solez K, Colvin RB, *et al*: The Banff 97 working classification of renal allograft pathology. *Kidney Int* 55:713–723, 1999
32. Rholl KS, Lee JKT, Ling D, *et al*: Acute renal rejection versus acute tubular necrosis in a canine model: MR evaluation. *Radiology* 160:113–117, 1986
33. Shapiro JI, Haug CE, Shanley PF, *et al*: Nuclear magnetic resonance study of renal allograft rejection in the rat. *Transplantation* 45:17–21, 1988
34. Bretan PN, Vigneron DB, Hricak H, *et al*: Assessment of in situ renal transplant viability by $^{31}$P-MRS: Experimental study in canines. *Am Surg* 59:182–187, 1993
35. Wang JJ, Hendrich KS, Jackson EK, *et al*: Perfusion quantitation in transplanted rat kidney by MRI with arterial spin labeling. *Kidney Int* 53:1782–1791, 1998
36. Winsett MZ, Amparo EG, Fawcett HD, *et al*: Renal transplant dysfunction: MR evaluation. *Am J Roentgenol* 150:319–323, 1988
37. Hanna S, Helenon O, Legendre C, *et al*: MR imaging of renal transplant rejection. *Acta Radiol* 32:42–46, 1991
38. Liou JT, Lee JK, Heiken JP, *et al*: Renal transplants: Can acute rejection and acute tubular necrosis be differentiated with MR imaging? *Radiology* 179:61–65, 1991
39. Szolar DH, Preidler K, Ebner F, *et al*: Functional magnetic resonance imaging of human renal allograft during the post transplant period: Preliminary observations. *Magn Reson Imaging* 15:727–735, 1997

40. Preidler KW, Szolar DH, Schreyer H, *et al*: Differentiation of delayed kidney graft function with gadolinium DTPA enhanced magnetic resonance imaging and Doppler ultrasound. *Invest Radiol* 31:364–371, 1996
41. Hricak H, Terrier F, Demas B: Renal allografts: Evaluation by MR imaging. *Radiology* 159:435–441, 1986
42. Sharma RK, Gupta RK, Poptani H, *et al*: The magnetic resonance renogram in renal transplant evaluation using dynamic contrast enhanced MR imaging. *Transplantation* 59:1405–1409, 1995
43. Soots A, Lautenschlager I, Krogerus L, *et al*: An experimental model of chronic renal allograft rejection in the rat using triple drug immunosuppression. *Transplantation* 65:42–46, 1998